Materials Research Express

PAPER

Influence of modified carbon substrate on boron doped ultrananocrystalline diamond deposition

Materials Research Express

RECEIVED
15 December 2017

REVISED
17 January 2018

ACCEPTED FOR PUBLICATION
25 January 2018

PUBLISHED
9 February 2018

PAPER

Influence of modified carbon substrate on boron doped ultrananocrystalline diamond deposition

Silvia Sizuka Oishi[1], Lilian Mieko Silva[1], Edson Cocchieri Botelho[2], Mirabel Cerqueira Rezende[3], Carlos Alberto Alves Cairo[4] and Neidenêi Gomes Ferreira[1]

[1] LAS, Instituto Nacional de Pesquisas Espaciais (INPE), Av. dos Astronautas 1758, São José dos Campos-SP, 12227-010, Brasil
[2] Departamento de Materiais e Tecnologia, Univ Estadual Paulista (UNESP), Av. Dr Ariberto Pereira da Cunha 333, Guaratinguetá-SP, 12516-410, Brasil
[3] Instituto de Ciência e Tecnologia, Universidade Federal de São Paulo (UNIFESP), Rua Talim 330, São José dos Campos-SP, 12231-280, Brasil
[4] Divisão de Materiais/Instituto de Aeronáutica e Espaço, AMR/IAE/DCTA—São José dos Campos, São Paulo 12228-904, Brazil

E-mail: silviaoishi@uol.com.br

Keywords: reticulated vitreous carbon, ultrananocrystalline diamond, HFCVD

Supplementary material for this article is available online

Abstract

Boron doped ultrananocrystalline diamond (B-UNCD) growth was studied on modified reticulated vitreous carbon (RVC) produced from poly(furfuryl alcohol) (PFA) resin with sodium hydroxide additions at two different heat treatment temperatures. The different amounts of NaOH in PFA (up to reaching pH values of around 3, 5, 7, and 9) aimed to neutralize the acid catalyst and to increase the PFA storage life. Besides, this procedure was responsible for increasing the oxygen content of RVC samples. Thus, the effect of carbon and oxygen coming from the substrates in addition to their different graphitization indexes on diamond morphology, grain size, preferential growth and boron doping level were investigated by FEG-SEM, x-ray diffraction and Raman spectroscopy. Therefore, B-UNCD films were successfully grown on RVC with pH values of 3, 5, 7, and 9 heat treated at 1000 and 1700 °C. Nonetheless, the higher oxygen amount during B-UNCD growth for samples with pH 7 and 9 heat treated at 1000 °C was responsible for the RVC surface etching and the decrease in the boron concentration of such samples. The cross section images showed that B-UNCD infiltrated at around 0.9 mm in depth of RVC samples while carbon nanowalls were observed mainly on RVC samples heat treated at 1000 °C for all pH range studied.

1. Introduction

Different types of substrates have been used for diamond growth to evaluate the influence of several parameters on film deposition. Specifically, the use of glassy carbon as substrate for diamond film deposition was systematically studied by Terranova *et al* [1–3], in which they showed the formation of an intermediate turbostratic graphite layer between the substrate and diamond film that enhanced diamond nucleation due to the etching resistance of this graphitized layer. Also, the etching of a graphitized layer generates a decrease in the sizes of graphitic regions and produces sp^3 sites that act as diamond precursor. Regardless of the substrate, the mechanism for the diamond growth by chemical vapour deposition can be generalized for micro, nano and ultrananocrystalline diamond [4, 5]. In all cases, the concentration of atomic H above the substrate must be large to drive all the H abstraction reactions. Depending on the gas mixture, reaction conditions used and substrate properties, the relative concentrations of H atoms, CH_3 radicals, and C_1 species (i.e. C, CH, and CH_2) near the substrate determine the probability of a renucleation event occurring and hence the morphology of the film [4, 5]. In the case of microcrystalline (MCD) and nanocrystalline diamond (NCD) growth, a H_2 rich gas mixture is used, but specifically for NCD, a higher CH_4/H_2 ratio to increase nucleation density or low growth temperature is required [6]. UNCD has been grown using $CH_4/H_2/Ar$ gas mixture with excess of argon which

Table 1. Sample nomenclatures.

PFA resin pH value	HTT	RVC nomenclature	Composite nomenclature
pH 3	1000	RVC3-1000	B-UNCD/RVC3-1000
pH 5	1000	RVC5-1000	B-UNCD/RVC5-1000
pH 7	1000	RVC7-1000	B-UNCD/RVC7-1000
pH 9	1000	RVC9-1000	B-UNCD/RVC9-1000
pH 3	1700	RVC3-1700	B-UNCD/RVC3-1700
pH 5	1700	RVC5-1700	B-UNCD/RVC5-1700
pH 7	1700	RVC7-1700	B-UNCD/RVC7-1700
pH 9	1700	RVC9-1700	B-UNCD/RVC9-1700

favors the formation of C_1 species resulting in a high rate of renucleation [5]. More recently, Zeng *et al* [7] showed that it is possible synthesize UNCD with H-rich/Ar-lean and high CH_4/H_2 ratio by using a chamber pressure <15 Torr.

Particularly, the carbon substrate tends to act as a carbon source and change the hydrocarbon/hydrogen ratio. Several papers have shown that it is possible to produce diamond through hydrogen etching of a solid carbon source [8–11]. Oxygen may also influence the chemical reactions leading to the consumption of some carbon species that reduce the diamond growth rate [12] or even may removes non-diamond carbon [13]. Reticulated vitreous carbon (RVC) can be considered a promising material for electrochemical applications and its use as substrate for micro and nanocrystalline diamond has already been studied by our group [14, 15]. For example, Baldan *et al* [14] have studied microcrystalline diamond growth on RVC with different graphitization indexes. They showed that RVC heat treated at 2000 °C presented the highest diamond nucleation since at this heat treatment temperature (HTT) the material becomes more resistant to the hydrogen etching. On the other hand, for RVC heat treated at 1000 °C diamond film presented the smallest grain size and growth rate attributed to the etching promoted by OH due to the high oxygen content in this substrate. Recently, Marton *et al* [16] have deposited boron doped diamond on graphite foam using a hot filament chemical vapor deposition (HFCVD) reactor and they also obtained different carbon nanomaterials depending on the deposition temperature, the foam porosity, and the distance from the heated filaments.

In a previous paper [17], the poly(furfuryl alcohol) (PFA) resin was neutralized with different amounts of sodium hydroxide up to reaching pH values of around 3, 5, 7, and 9. Then, RVC samples were processed using these modified resins and heat treated at 1000 and 1700 °C. RVC samples processed from PFA with pH 3 and 5 heat treated at 1000 and 1700 °C were considered the most ordered structurally as was extensively discussed in our previous paper [17]. This work aimed to study the influence of RVC with modified matrix (i.e. from PFA with different pH values and different graphitization indexes) on the B-UNCD/RVC properties as well as regarding the concomitant growth of other carbon materials deposited on the interior of this 3D structure. RVC modified matrixes have different proportions of carbon and oxygen, but sodium may appear in the atomic composition for samples processed from PFA with pH values of 7 and 9. There are several studies showing the effect of oxygen addition on diamond formation [13, 18–20], but the effect of oxygen coming from RVC in the B-UNCD growth has not been explored yet. In this work, B-UNCD films were grown by hot filament chemical vapour deposition (HFCVD) technique using CH_4, H_2 and Ar. The films were characterized by field emission scanning gun electron microscopy (FEG-SEM), x-ray diffraction (XRD), and Raman spectroscopy. B-UNCD/RVC cross section of each sample was examined in depth only by FEG-SEM. This study allows extending the possible applications of B-UNCD/RVC composites by understanding the composition inside their 3D arrangement not to mention their different morphological and structural properties.

2. Experimental

RVC samples were processed from PFA resin with different amounts of concentrated sodium hydroxide solution until the resin reached pH values of around 3, 5, 7 and 9. The samples nomenclature was created depending on the pH values of the PFA resin (RVC 3, 5, 7 or 9), followed by their related RVC HTT (1000 or 1700 °C) as presented in table 1. After impregnation of polyurethane foams by modified resins catalyzed with 3 wt% of diluted p-toluenesulfonic acid (60 wt%), these samples were cured and heat treated at 1000 and 1700 °C. Concerning the RVC pore size used in this work (about 70 pores per inch), it is in the average grade of RVC used as electrode with successes for electrochemical applications. The synthesis of PFA resin and RVC processing were detailed in [17, 21]. For B-UNCD deposition, RVC samples were first prepared using seeding pretreatment to improve the diamond nucleation process. In this step, RVC substrates were immersed in a solution containing 0.25 μm of diamond particles dispersed in hexane solvent, followed by ultrasonic agitation

for 2 h. This time was chosen as the most appropriate because it resulted in a more uniform spread diamond seed throughout the stems and depth compared to that of other times (1 h and 1 h 30 min) as previously verified. Ultrananocrystalline diamond films were grown by HFCVD technique, using 5 filaments of tungsten with 125 μm diameter, placed at 6 mm of sample top and 18 h deposition time. Reactor pressure and the substrate temperature were kept at 4 kPa and 680 °C, respectively, with a gas mixture composed of 80% Ar, 19% H_2 and 1% CH_4 in a total flow of 150 sccm. In general, UNCD has been deposited at Ar concentration above 90% [4, 22, 23], however, with 80% Ar, B-UNCD could be obtained on RVC matrix. The boron doping was performed by additional hydrogen line passing through a bubbler containing B_2O_3 dissolved in methanol with B/C ratio of 30 000 ppm. B-UNCD/RVC composites morphologies were evaluated by FEG-SEM using a Tescan Mira3 at an accelerating voltage of 15 kV or 20 kV. The quality of the films and the boron concentration were evaluated with a Raman scattering spectroscopy LabRAM HR evolution from Horiba Scientific, using 514.5 nm line of argon ion laser. The x-ray diffraction patterns were used to investigate the B-UNCD grain size and the intensity ratio I_{220}/I_{111} using a PANanalytical model X'Pert Pro MPD diffractometer with the CuKα radiation ($\lambda = 1.54$ Å) using θ–2θ scan from 5° to 100°.

3. Results and discussion

3.1. Morphological analyses

In previous paper, the use of microcrystalline diamond (MCD) growth conditions in RVC matrix resulted in different diamond morphologies depending on the growth time, sample depth, and RVC graphitization index [14, 15]. For example, using a typical gas mixture of 1% CH_4 in H_2, MCD was obtained on the RVC surface, but in deeper regions (at about 1.5 mm from sample top), NCD was deposited as a result of poor concentration of atomic hydrogen [15]. In this work, B-UNCD was grown using Ar-rich gas mixture on modified RVC surface. For the sake of simplicity, figure 1 shows representative micrographs with low magnification (100x) of B-UNCD grown on RVC top surface followed by the lowest and the highest pH values studied, named as: B-UNCD/RVC3-1000, B-UNCD/RVC3-1700, B-UNCD/RVC9-1000 and B-UNCD/RVC9-1700. The other results concerning B-UNCD/RVC5 and B-UNCD/RVC7 can be found in the supplementary material. The samples heat treated at 1000 °C, B-UNCD/RVC3-1000 (figure 1(a)) and B-UNCD/RVC5-1000 (figure S1(a) is available online at stacks.iop.org/MRX/5/026405/mmedia) present a good coverage with B-UNCD film, despite the fact that some etching by hydrogen or oxygen is inevitable. The inset of figure 1(a) shows a higher magnification (2000×) of a stem, where it is possible to identify cauliflower structures and a smooth morphology characteristic of UNCD. The inset of figure S1(a) (enlarged area of the concavity indicated by the arrow) seems to present an etched region, but a more detailed analysis shows the presence of nanocrystalline graphite platelets or carbon nanowalls (CNW) as already reported by some authors [6, 24, 25]. The use of CVD technique has been fairly applied for obtaining CNW that usually grows on a poor hydrogen or even in hydrogen free environments and temperature at around 500 °C. Sample B-UNCD/RVC7-1000 (figure S1(c)) presents some etched areas similarly to those for sample B-UNCD/RVC9-1000 (figure 1(c)). These samples present the highest oxygen contents as defined according to [17], i.e., 7.85% for B-UNCD/RVC7-1000 and 21.45% for B-UNCD/RVC9-1000 in comparison to 4.65% for B-UNCD/RVC3-1000 and 6.41% for B-UNCD/RVC5-1000. The oxygen is responsible for OH formation that is more efficient to etch carbon surface than atomic hydrogen as already discussed in previous papers [14, 23]. The insets of figures S1(c) and 1(c) show these etched areas with higher magnification (2000×). Increasing HTT up to 1700 °C, the RVC with different pH values present closer oxygen content, i.e., 2.16, 1.19, 1.82, and 1.40% for RVC3-1700, RVC5-1700, RVC7-1700, and RVC9-1700, respectively [17]. In general, samples B-UNCD/RVC3-1700 and B-UNCD/RVC5-1700 present regions without etching and with higher secondary nucleation (as shown in the insets of figures 1(b) and S1(b), respectively) in comparison to those for samples heat treated at 1000 °C. The B-UNCD films of RVC7-1700 and RVC9-1700 are more continuous than those of samples heat treated at 1000 °C (as presented in figures S1(d) and 1(d), respectively). However, carbon etching occurs after B-UNCD formation leaving holes or just the B-UNCD shell after full gasification of the carbon substrate, as demonstrated in figures S1(d) and 1(d) insets. In this case, for RVC7-1700 and RVC9-1700 samples, where oxygen from substrate has decreased after 1700 HTT, diamond grows faster than carbon etching showing the substrate inertia due to its more ordered structure. However, the long growth time allowed atomic hydrogen to etch carbon substrate leaving the B-UNCD shell after full carbon gasification. This process is probably related to an increase in the C-OH and COOH surface groups and to the fragile structure that remained after the great oxygen and sodium losses during 1700 HTT of mainly RVC9 sample, leaving a porous and a rough surface as reported in [17].

B-UNCD/RVC cross-section images allow observing the film growth in depth and verifying the internal RVC structure. These images were schematically divided considering two layers and the materials observed in each layer are depicted in figure 2. Firstly, the modified substrates heat treated at 1000 °C will be discussed.

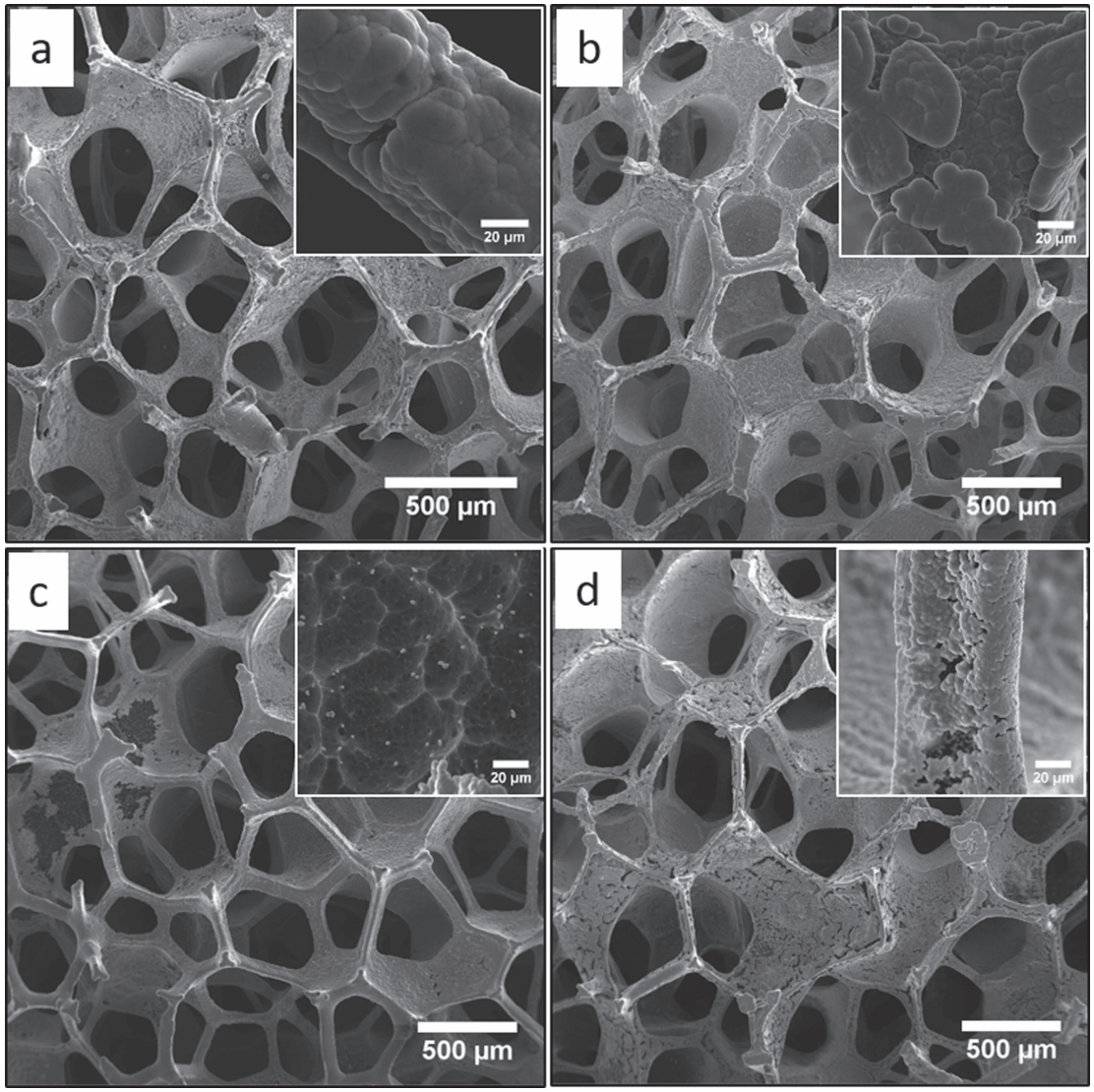

Figure 1. FEG-SEM representative images of: (a) B-UNCD/RVC3-1000, (b) B-UNCD/RVC3-1700, (c) B-UNCD/RVC9-1000, and (d) B-UNCD/RVC9-1700. The insets show the images with higher magnification (2000×).

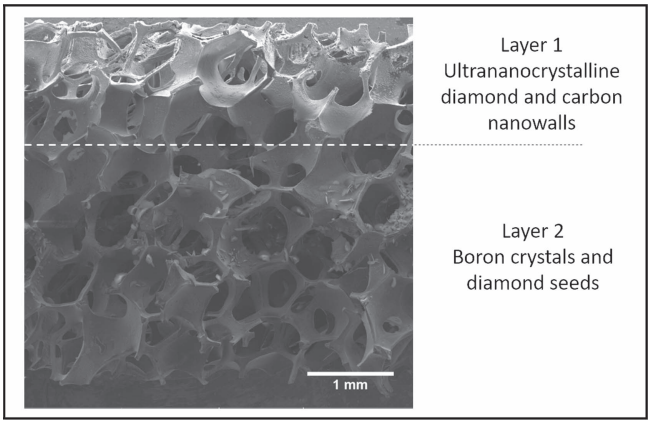

Figure 2. B-UNCD/RVC9-1000 cross-section images considering two layers in depth.

Figure 2 shows the B-UNCD/RVC9-1000 sample, where the RVC9-1000 substrate presents the highest amounts of oxygen and sodium. However, all samples heat treated at 1000 °C showed a similar growth pattern in depth, i.e., B-UNCD and carbon nanowalls in Layer 1 as well as boron crystals and diamond seeds in Layer 2.

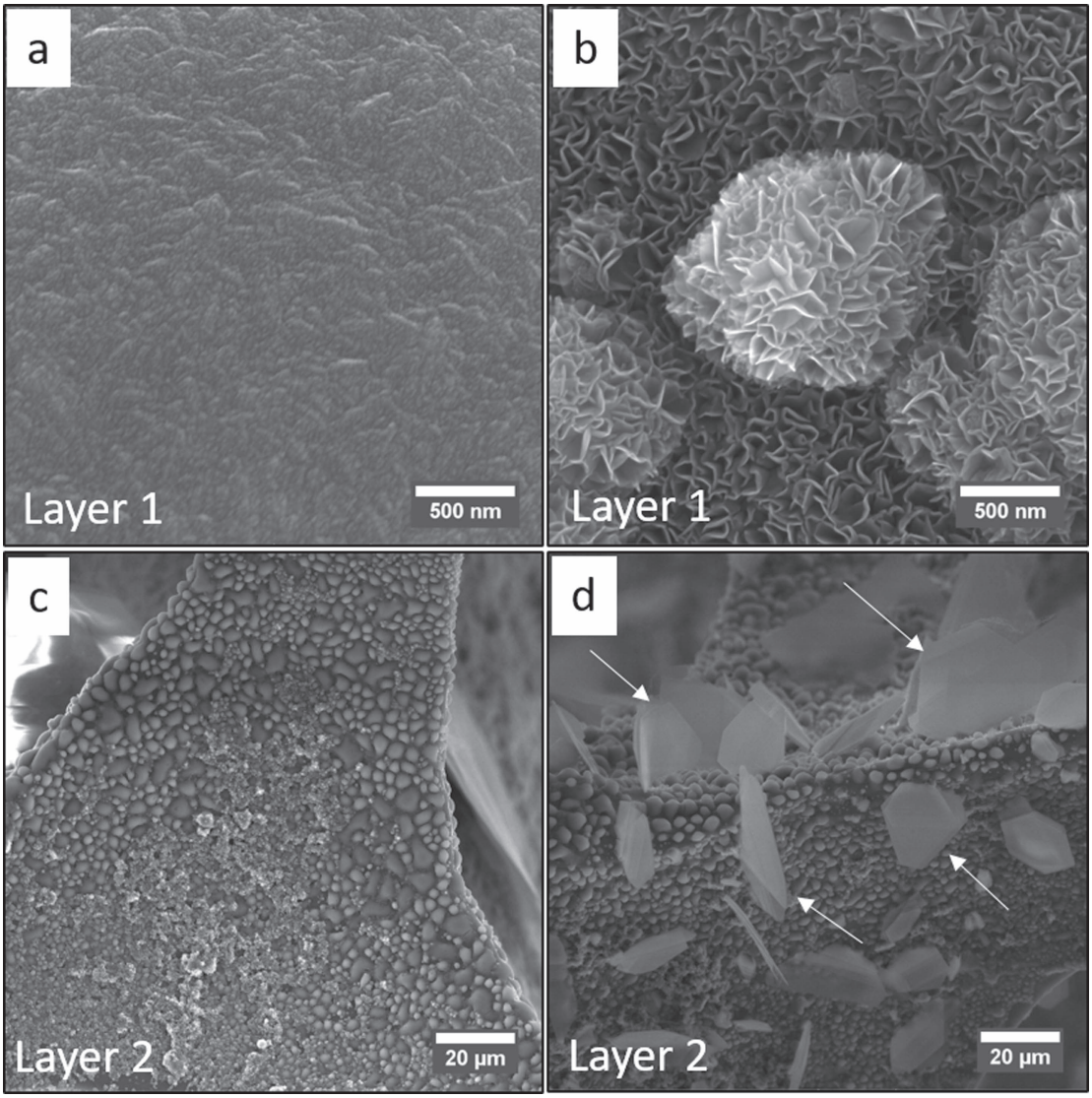

Figure 3. FEG-SEM images of materials presented on Layer 1 and Layer 2 of B-UNCD/RVC9-1000 sample cross section: (a) B-UNCD, (b) CNW, (c) surface with bubbles, and (d) boron oxide crystals pointed by arrows.

For a more detailed explanation, figure 3 presents Layer 1 and Layer 2 topographic images of B-UNCD/RVC9-1000 in higher magnifications, where the B-UNCD film penetrates at around 0.9 mm depending on the alveoli opening. Nevertheless, regardless of the substrate pH value, the in depth growth reached at around 0.9 mm for all samples. The diamond coating is deep enough since we are growing a nanostructure, therefore, this depth is seven orders of magnitude higher than the crystals sizes. Probably, UNCD in depth growth is restricted by the addition of high percentage of argon that reduces the substrate temperature since its thermal conductivity is 10.5 times lower than that of hydrogen. Hence, the heat transfer from the filament to the substrate is much more effective at high hydrogen concentrations [26]. In this sense, probably MCD could grow deeper, but this consideration require further investigation. Figure 3(a) shows a higher magnification film image (100 kx) which enables identifying B-UNCD clusters that are aggregates of diamond grains resulting from a high renucleation rate [7, 27]. Another nanostructure observed in Layer 1 is the carbon nanowalls (CNW) (figure 3(b)). These nanostructures are mainly found in the RVC concavities as previously shown in figure S1(a) inset. They have been observed by Kim *et al* [24] when depositing UNCD by microwave plasma-assisted CVD on glassy carbon powder using similar gas mixture (1% CH_4/7% H_2/92% Ar). Barbosa *et al* [6] have also identified lamellas of graphite on silicon substrate obtained by HFCVD from 1% CH_4/9% H_2/90% Ar gas mixture at higher substrate temperature of 850 °C.

The second layer (Layer 2) of B-UNCD/RVC9-1000 sample cross section has, as main features, the presence of bubbles on the stem surfaces and boron oxide crystals as shown in figures 3(c), (d), respectively. The rough surface with bubble shape observed only on sample RVC9-1000 is probably formed by the volatiles released by this substrate. RVC9-1000 substrate presents the highest atomic percentage of oxygen in its structure as showed

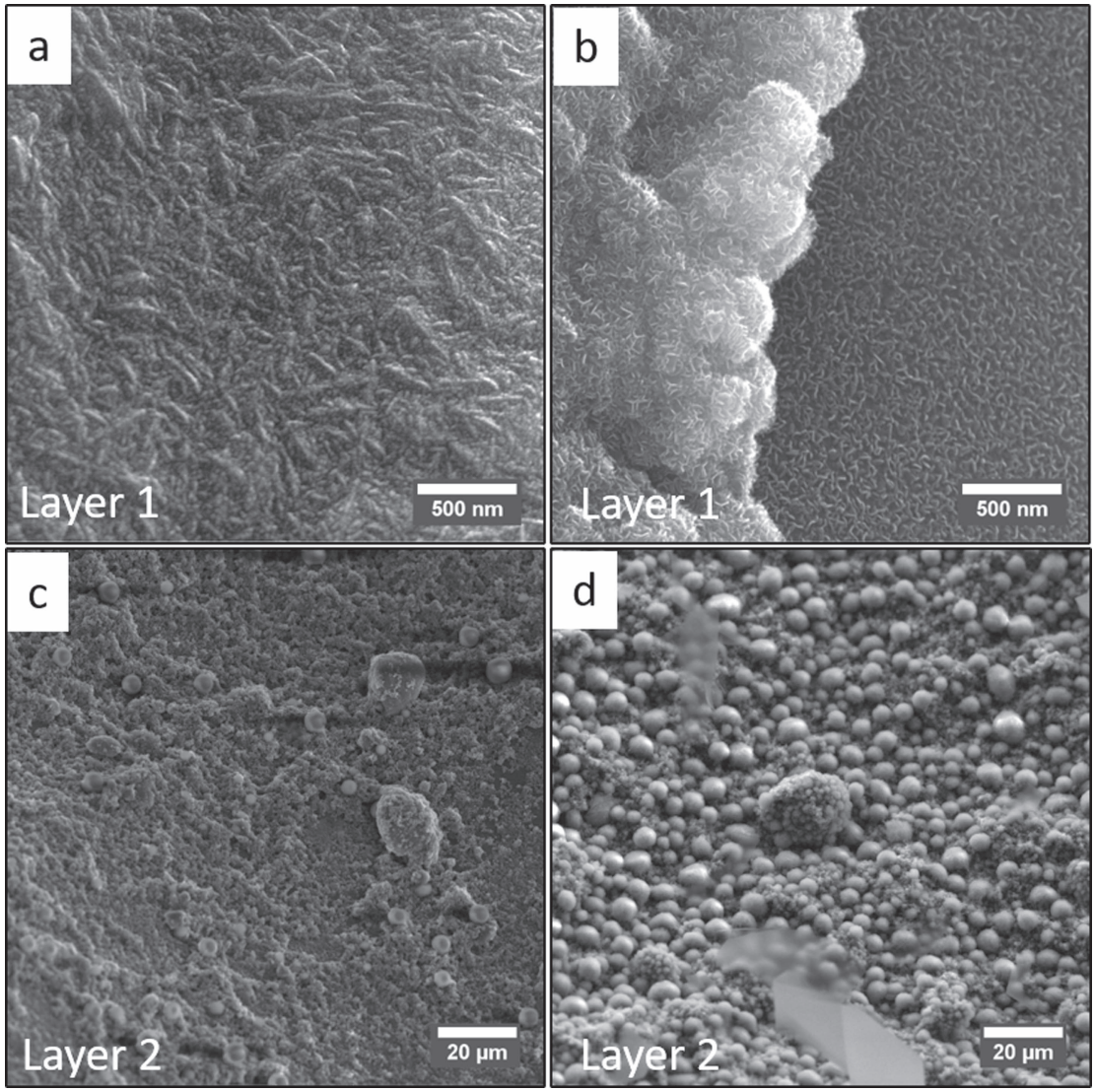

Figure 4. FEG-SEM images of materials presented on Layer 1 and Layer 2 of B-UNCD/RVC9-1700 sample: (a) B-UNCD, (b) initial formation of CNW growth, (c) diamond seeds, and (d) boron oxide with ball and crystal shape.

in previous paper (21.45%) [17]. Therefore, during diamond growth the substrate releases these volatiles and a portion of them precipitates forming the bubbles. These bubble formations were also observed in the literature at low substrate HTT [28]. The presence of boron crystals was confirmed by energy dispersive x-ray spectroscopy (EDS) of the circled area presented in figure S2(a), which refers to B-UNCD/RVC7-1000 sample. The boron trioxide initially dissolved in methanol is carried by the hydrogen and when the gas passes inside the RVC, its lower temperature crystallizes the boron trioxide. EDS analysis (figure S2(b)) demonstrates the possible presence of B_2O_3, NaOH, and some oxygen from the substrate. These crystals are more evident on samples B-UNCD/RVC7-1000 and B-UNCD/RVC9-1000, while sample B-UNCD/RVC3-1000 presents spheres of boron oxide besides crystals (figures S3(a), (b)), which are molded by the continuous gas flow into the RVC concavities. figure S3(b) shows a sphere with higher magnification where it is possible to observe that it was created from crystallized boron oxide fibers.

For comparison, to explore the cross section of B-UNCD/RVC heat treated at 1700 °C, we consider the same division into two layers of B-UNCD/RVC9-1700 sample. For Layer 1, the characteristic UNCD grain morphologies at the top sample (figure 4(a)) and regions which seem to be the initial formation of CNW structures with the sponge appearance can be highlighted, as shown in figure 4(b). For Layer 2, mainly diamond seeds (figure 4(c)) and boron oxide in ball shape (figure 4(d)) can be identified. Some boron oxide crystals appeared only on sample B-UNCD/RVC9-1700 in small amounts. Therefore, morphological analyses showed that the higher structural ordering of RVC1700 in comparison to that of RVC1000 samples increased the matrix inertia against carbon etching and CNW formation.

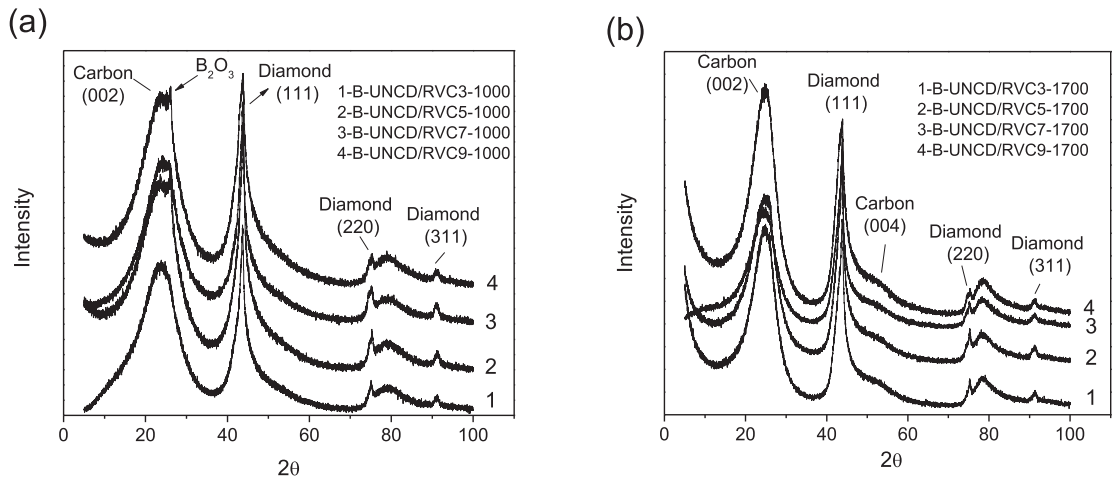

Figure 5. XRD patterns of B-UNCD/RVC composites: (a) B-UNCD/RVC1000 and (b) B-UNCD/RVC1700 processed from PFA with different pH values.

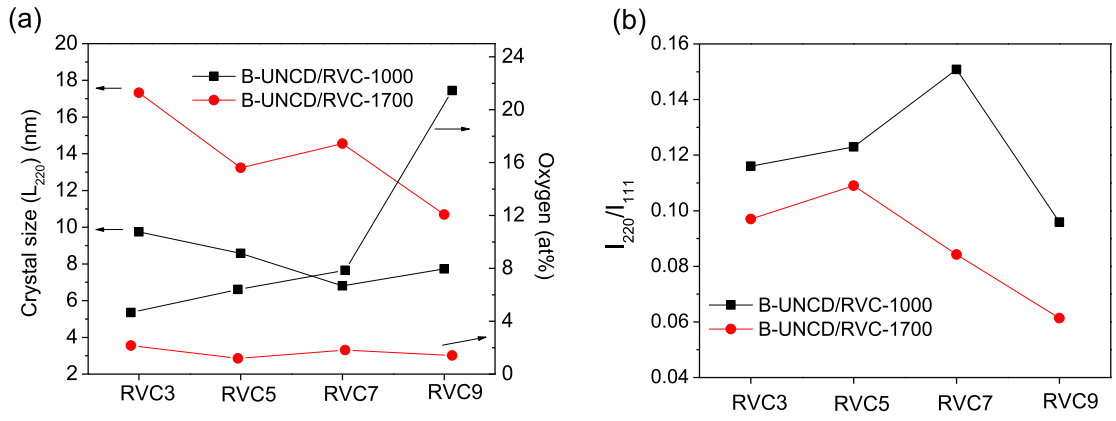

Figure 6. (a) Crystal size of B-UNCD grown on different RVC samples and oxygen content in each RVC sample and (b) relative intensity ratio I_{220}/I_{111} of B-UNCD.

3.2. XRD and Raman spectroscopy characterizations of B-UNCD films

The XRD patterns of B-UNCD/RVC-1000 and B-UNCD/RVC-1700 samples are presented in figures 5(a), (b), respectively. The NCD peaks detected for all samples at $2\theta = 44.0, 75.4$ and 91.4° can be identified as the (111), (220) and (311) reflections of diamond, respectively. The peak at $2\theta = 27.0^\circ$ is related to the boron oxide and it can be overlapped by the carbon band (002) after 1700 °C HTT due to the increase of this band intensity. An increase in HTT also lead to the appearance of (004) band as a shoulder at 53.0°. Figure 6 presents the results of crystal size and preferential crystal growth (I_{220}/I_{111}) of B-UNCD grown on different RVC substrates. Since the (100) carbon band is overlapping the (111) diamond peak and affecting the bandwidth as it can be clearly seen in figures S4(a), (b) (suplementar material), the average crystal sizes were calculated from (220) diamond peak using the Scherrer equation [29].

The crystal size for B-UNCD grown on RVC-1000 samples varies from 9.7 nm (B-UNCD/RVC3-1000) to 6.8 nm (B-UNCD/RVC7-1000) while for RVC-1700 samples all B-UNCD crystal sizes present a substantial increase in comparison to those for RVC-1000 samples at the same pH value, varying from 17.3 nm (B-UNCD/RVC3-1700) to 10.7 nm (B-UNCD/RVC9-1700). The grain size difference generated by the substrate HTT can be associated to the contribution of carbon substrate to diamond growth. RVC microstructure heat treated at 1000 °C is more susceptible to hydrogen etching which increase the carbon gasified during diamond growth and leads to a grain size reduction. Also, the oxygen presence favored the OH and CO formation. As previously remarked, the OH formation inevitably promotes the etching of carbon surface producing CO as a stable specie that decreases the growth rate [14]. The RVC7-1000 sample presents the highest disorder [17] and the lowest grain size among the RVC-1000 samples, which clearly shows that the RVC microstructure contribution has greater influence than that of oxygen presence to this sample grain size. The oxygen contribution to diamond

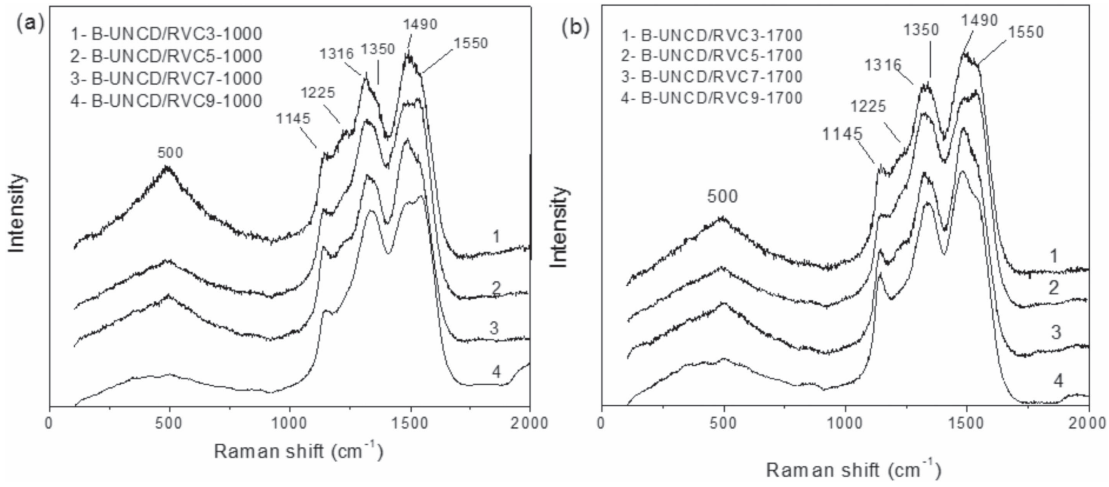

Figure 7. Raman spectra of (a) B-UNCD/RVC-1000 and (b) B-UNCD/RVC-1700. The spectra have been offset vertically for clarity.

growth has already been investigated. For example, Gicquel *et al* [19] observed that concentrations of O_2 above 0.2% decrease the grain size and the nucleation density using a HFCVD reactor. Ting and Shih [30], also noticed a decrease in grain size when increasing oxygen concentration on diamond growth using a microwave plasma enhanced CVD technique. On the other hand, Das *et al* [20] observed an enhancement in growth rate and an increase in diamond grain size with 0.75% O_2 using microwave plasma enhanced CVD system at low deposition temperature (450 °C). Nonetheless, the oxygen contribution from the substrate to diamond grain size can be considered minimal for RVC9-1000 sample, which has the highest oxygen content (21.4%) and presents the small change in its grain size. In addition, after 1700 °C HTT, the oxygen content is similar among samples with different pH values, but a greater variation in grain size is observed. These results confirm that the contribution of gasified carbon is more relevant than that of the oxygen from the substrate. Thus, the increase in the substrate structural organization decreases its reactivity and, consequently, increases the diamond crystal size. Therefore, RVC3-1700 sample as the most organized sample exhibit the highest crystal size. The lowest crystal size of RVC9-1700 sample can be related to the greater contribution of gasified carbon from the substrate that was previously evidenced by the SEM images of the etched sample (figure 1(d)-inset) probably because of the higher quantity of C-OH and COOH groups on the surface in relation to other RVC-1700 samples [17].

The intensity ratio I_{220}/I_{111} shows the preferential growth in a polycrystalline diamond film. For randomly oriented diamond powders this ratio is 0.25 [31]. All samples present I_{220}/I_{111} ratio below this value, which indicates that the films are ultrananocrystalline dominated by [111] texture. The (111) planes are oxidized more easily than (220) planes [32], therefore, the oxygen in the boron source as well as in the methanol, which is used to dissolve the B_2O_3, and even the oxygen from the substrate may contribute to this oxidation. According to Li *et al* [33], when a high level of boron doping is used, the [111] texture is dominant, as it can also be observed in this work. B-UNCD films grown on RVC-1000 present higher I_{220}/I_{111} ratio than their respective films grown on RVC-1700. This fact is well correlated with the faster growth rate of (220) planes for UNCD films that exhibit a large grain boundary density due to their small grain size and large non-diamond phase [34]. Nonetheless, RVC9-1000 and RVC9-1700 samples display the lowest values of I_{220}/I_{111} ratio in comparison to those of other samples with the same HTT. Due to the higher oxygen content in the substrate associated with the lower diamond grain size, it is expected that nanometric (220) plane develops faster than the others. In this case, the results differ from the literature and we conclude that the oxygen from the substrate is reacting with the boron, decreasing both substances in the system, which favorably leads to a predominant [111] texture [33, 35].

Raman measurements were performed only on B-UNCD samples in three different regions, since the Raman spectra of RVC substrate with different pH values were already explored in previous paper [17]. Figure 7 presents the Raman spectra of B-UNCD grown on different RVC surfaces. The spectra were normalized with respect to the higher intensity band for better visualization of all bands. The spectra depict similar features to those obtained on the literature [36, 37], such as: a diamond peak shifted to lower wavenumbers (at around 1320 cm^{-1}) overlapped by the D band at 1350 cm^{-1}; the bands at 1150 and 1490 cm^{-1} related to the transpolyacetylene segments at the grain boundaries of the ultrananocrystalline diamond surface; the band at 1550 cm^{-1} assigned to G band; and the bands at 500 and 1220 cm^{-1}, related to the boron doping. The down-shifting of diamond peak compared to the microcrystalline diamond peak (1332 cm^{-1}) is related to the Fano interference and this shift increases toward lower wavenumbers with increasing boron doping [36]. As can be

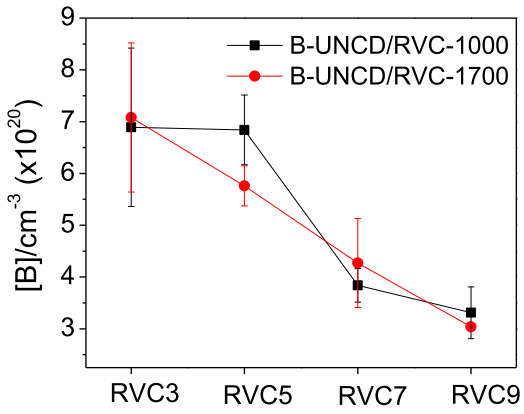

Figure 8. Boron concentration of B-UNCD/RVC composites.

seen, there is no significant difference between the spectra of B-UNCD samples grown on RVC-1000 and RVC-1700.

The presence of the band at 500 cm^{-1} is attributed to an increase in the concentration of boron pairs that have local vibration modes producing this wide peak that varies with the amount of boron incorporation [38]. This wide peak can be fitted by the sum of a Gaussian and a Lorentzian component. The boron concentration can be estimated by the wavenumber position, ω, of the Lorentzian component, as presented in equation (1) [39]. Where ω is in cm^{-1} and the boron concentration, [B], is in the range from 2×10^{20} to 1×10^{22} cm^{-3}.

$$[B]/cm^{-3} = 8{,}44 \times 10^{30} \exp(-0.048\omega) \quad (1)$$

Equation (1) measures only substitutional boron atoms and it underestimates their concentration in the NCD films by a factor of around 5 [39]. May *et al* [39], showed that doping efficiency for MCD films is greater than that for NCD, suggesting that a significant amount of boron is being incorporated at the grain boundaries.

The boron concentration (figure 8) present a small variation among different samples and it is in the range from 7.1×10^{20} to 3.0×10^{20} boron/cm^3. As the RVC pH values increase, the boron incorporation decreases probably due to the consumption of some boron species by the oxygen from the substrate. RVC samples heat treated at 1700 °C follow similar trend of RVC-1000 samples considering the standard deviation. As the oxygen concentration is similar for RVC-1700 samples, it can be inferred that substrate etching of B-UNCD/RVC7-1700 and B-UNCD/RVC9-1700 samples also decrease the boron incorporation since diamond growth is reduced.

4. Conclusion

This study demonstrated that the use of RVC modified substrates at different HTT influenced the growth of B-UNCD as well as its morphology in the interior of RVC structure. According to FEG-SEM images, the substrates RVC3 and RVC5 heat treated at 1000 and 1700 °C were the best to B-UNCD growth, since they presented a good film coverage and little or no substrate etching in comparison to the films grown on RVC7 and RVC9 substrates heat treated at 1000 and 1700 °C. B-UNCD/RVC samples cross section showed that B-UNCD penetrates around 0.9 mm in the interior of all RVC samples. Carbon nanowalls growth was possible due to the poor hydrogen environment and they were observed mainly on RVC-1000 substrates. After increasing the RVC graphitization index the substrate became more stable and did not allow CNW nucleation. The contribution of gasified carbon to the diamond grain size is more relevant than that of the oxygen from the substrate because by increasing the RVC structural organization its reactivity decreases and the diamond crystal size increases. On the other hand, the contribution of the oxygen from the substrate can be verified mainly in the boron doping where at higher oxygen levels the boron concentration decreases.

Acknowledgments

The authors acknowledge São Paulo Research Foundation (FAPESP) grant numbers: 2014/27164-6 and 2016/13393-9, CNPq grant numbers: 162683/2013-8 and 302017/2015-1, and CAPES by the financial support.

ORCID iDs

Silvia Sizuka Oishi https://orcid.org/0000-0001-5540-3382

References

[1] Terranova M L, Polini R, Sessa V, Braglia M and Cocito G 1992 A study of diamond synthesis on glassy carbon by the hot filament chemical vapour deposition technique *Diam Relat Mater [Internet]* **1** 969–77

[2] Terranova M L, Rossi M, Sessa V and Vitali G 1996 Influence of different carbon structures on diamond synthesis by chemical vapour deposition *Phys. Status Solidi A-Applications Mater Sci.* **154** 127–40

[3] Terranova M L, Rossi M, Sessa V and Vitali G 1994 Development of different carbon phases during diamond film growth by CVD on glassy carbon substrates *Solid State Commun [Internet]* **91** 55–8

[4] May P W, Ashfold M N R and Mankelevich Y A 2007 Microcrystalline, nanocrystalline, and ultrananocrystalline diamond chemical vapor deposition: experiment and modeling of the factors controlling growth rate, nucleation, and crystal size *J. Appl. Phys.* **101** 1–9

[5] May P W and Mankelevich Y A 2006 Experiment and modeling of the deposition of ultrananocrystalline diamond films using hot filament chemical vapor deposition and $Ar/CH_4/H_2$ gas mixtures: a generalized mechanism for ultrananocrystalline diamond growth *J Appl Phys [Internet]* **100** 24301

[6] Barbosa D C, Almeida F A, Silva R F, Ferreira N G, Trava-Airoldi V J and Corat E J 2009 Influence of substrate temperature on formation of ultrananocrystalline diamond films deposited by HFCVD argon-rich gas mixture *Diam Relat Mater [Internet]* **18** 1283–8

[7] Zeng H *et al* 2015 Boron-doped ultrananocrystalline diamond synthesized with an H-rich/Ar-lean gas system *Carbon N Y.* **84** 103–17

[8] Silva W M, Ferreira N G, Travello J, Almeida E C, Azevedo A F and Baldan M R 2007 Dependence of diamond nucleation and growth through graphite etching at different temperatures *Diam. Relat. Mater.* **16** 1705–10

[9] Chow L, Wang H, Kleckley S, Schulte A and Casey K 1995 Diamond nucleation on graphite substrate using a pure hydrogen feed *Solid State Commun [Internet]* **93** 999–1002

[10] Woo H K, Lee S T, Lee C S, Bello I and Lam Y W 1997 Diamond films grown by hot filament chemical vapor deposition from a solid carbon source *J Vac Sci Technol A-Vacuum Surfaces Film.* **15** 2988–92

[11] Regel L L and Wilcox W R 2000 Deposition of diamond on graphite and carbon felt from graphite heated in hydrogen at low pressure *J. Mater. Sci. Lett.* **19** 455–7

[12] Migliorini F L, Alegre M D, Baldan M R, Lanza M R V and Ferreira N G 2014 Doped diamond electrodes on titanium substrates with controlled sp 2/sp3 hybridization at different boron levels *Thin Solid Films [Internet]* **564** 97–103

[13] Harris S J and Weiner A M 1989 Effects of oxygen on diamond growth *Appl. Phys. Lett.* **55** 2179–81

[14] Baldan M R, Ramos S C, Almeida E C, Azevedo A F and Ferreira N G 2008 Homogeneous micro and nanocrystalline diamond coating on reticulated vitreous carbon treated at different temperatures *Diam Relat Mater [Internet]* **17** 1110–5

[15] Diniz A V, Trava-Airoldi V J, Corat E J and Ferreira N G 2005 Micro and nanocrystalline diamond formation on reticulated vitreous carbon substrate *Chem. Phys. Lett.* **414** 412–6

[16] Marton M *et al* 2014 Deposition of boron doped diamond and carbon nanomaterials on graphite foam electrodes *Appl. Surf. Sci.* **312** 139–44

[17] Oishi S S, Botelho E C, Rezende M C and Ferreira N G 2017 Structural and surface functionality changes in reticulated vitreous carbon produced from poly(furfuryl alcohol) with sodium hydroxide additions *Appl. Surf. Sci. [Internet]* **394** 87–97

[18] Issaoui R, Achard J, Silva F, Tallaire A, Mille V and Gicquel A 2011 Influence of oxygen addition on the crystal shape of CVD boron doped diamond *Phys. Status Solidi Appl. Mater Sci.* **208** 2023–7

[19] Gicquel A, Héau C, Fabre D and Perrière J 1992 Processes and parameters for diamond deposition *Diam. Relat. Mater.* **1** 776–81

[20] Das D, Singh R N, Barney I T, Jackson A G and Mukhopadhyay S M 2008 Effect of oxygen on growth and properties of diamond thin film deposited at low surface temperature *J. Vac. Sci. Technol.* A **26** 1487–96

[21] Oishi S S, Rezende M C, Origo F D, Damião A J and Botelho E C 2013 Viscosity, pH, and moisture effect in the porosity of poly(furfuryl alcohol) *J. Appl. Polym. Sci.* **128** 1680–6

[22] Barbosa D C, Hammer P, Trava-Airoldi V J and Corat E J 2012 The valuable role of renucleation rate in ultrananocrystalline diamond growth *Diam Relat Mater [Internet].* **23** 112–9

[23] Medeiros L I, Couto A B, Matsushima J T, Baldan M R and Ferreira N G 2012 Nanocrystalline diamond coating on carbon fibers produced at different temperatures: morphological, structural and electrochemical study *Thin Solid Films [Internet]* **520** 5277–83

[24] Kim D Y, Merzougui B and Swain G M 2009 Preparation and characterization of glassy carbon powder modified with a thin layer of boron-doped ultrananocrystalline diamond (B-UNCD) *Chem. Mater.* **21** 2705–13

[25] Itoh T 2011 Synthesis of carbon nanowalls by hot-wire chemical vapor deposition *Thin Solid Films [Internet]* **519** 4589–93

[26] Baranauskas V, Peterlevitz A C, Ceragioli H J and Durrant S F 2001 Micro-crystalline diamond and nano-carbon structures produced using a high argon concentration in hot-filament chemical vapor deposition *J Vac Sci Technol A Vacuum, Surfaces, Film [Internet]* **19** 1057–62

[27] Wang S, Swope V M, Butler J E, Feygelson T and Swain G M 2009 The structural and electrochemical properties of boron-doped nanocrystalline diamond thin-film electrodes grown from Ar-rich and H2-rich source gases *Diam Relat Mater [Internet]* **18** 669–77

[28] Gonçalves E S, Rezende M C, Takahashi M F K and Ferreira N G 2006 Electrochemical reversibility of reticulated vitreous carbon electrodes heat treated at different carbonization temperatures *Mater Res.* **9** 147–52

[29] Heiman A, Lakin E, Zolotoyabko E and Hoffman A 2002 Microstructure and stress in nano-crystalline diamond films deposited by DC glow discharge CVD *Diam Relat Mater [Internet].* **11** 601–7

[30] Ting J M and Shih W 2001 Growth kinetics of diamond film on diamond composite materials *Mater. Chem. Phys.* **72** 185–90

[31] Kulisch W *et al* 2012 Low temperature growth of nanocrystalline and ultrananocrystalline diamond films: a comparison *Phys Status Solidi [Internet]* **209** 1664–74

[32] Sun C Q 2003 Oxidation electronics: bond-band-barrier correlation and its applications *Prog. Mater. Sci.* **48** 521–685

[33] Li H *et al* 2010 Investigation on crystalline structure, boron distribution, and residual stresses in freestanding boron-doped CVD diamond films *J Cryst Growth [Internet]* **312** 1986–91

[34] Haque M S, Naseem H A, Malshe A P and Brown W D 1997 A study of stress in microwave plasma chemical vapor deposited diamond films using x-ray diffraction *Chem. Vap Depos.* **3** 129–35

[35] Wang X, Zhao T, Sun F and Shen B 2015 Comparisons of HFCVD diamond nucleation and growth using different carbon sources *Diam Relat Mater [Internet]* **54** 26–33

[36] Gajewski W *et al* 2009 Electronic and optical properties of boron-doped nanocrystalline diamond films *Phys. Rev. B—Condens Matter Mater Phys.* **79** 1–14
[37] Azevedo A F, Baldan M R and Ferreira N G 2012 Nanodiamond films for applications in electrochemical systems *Int J Electrochem [Internet]* **2012** 1–16
[38] Bernard M, Baron C and Deneuville A 2004 About the origin of the low wave number structures of the Raman spectra of heavily boron doped diamond films *Diam. Relat. Mater.* **13** 896–9
[39] May P W, Ludlow W J, Hannaway M, Heard P J, Smith J A and Rosser K N 2008 Raman and conductivity studies of boron-doped microcrystalline diamond, facetted nanocrystalline diamond and cauliflower diamond films *Diam. Relat. Mater.* **17** 105–17